Resistance mechanisms to TP53-MDM2 inhibition identified by in vivo piggyBac transposon mutagenesis screen in an $Arf^{-/-}$ mouse model

Emilie A. Chapeau[a,1], Agnieszka Gembarska[a,2], Eric Y. Durand[a,2], Emeline Mandon[a], Claire Estadieu[a], Vincent Romanet[a], Marion Wiesmann[a], Ralph Tiedt[b], Joseph Lehar[c], Antoine de Weck[a], Roland Rad[d,e], Louise Barys[b], Sebastien Jeay[a], Stephane Ferretti[a], Audrey Kauffmann[a], Esther Sutter[f], Armelle Grevot[f], Pierre Moulin[f], Masato Murakami[a], William R. Sellers[c], Francesco Hofmann[a], and Michael Rugaard Jensen[a]

[a]Oncology Disease Area, Novartis Institutes for BioMedical Research, 4056 Basel, Switzerland; [b]Oncology Translational Research, Novartis Institutes for BioMedical Research, 4056 Basel, Switzerland; [c]Oncology Disease Area, Novartis Institutes for BioMedical Research, Cambridge, MA 02139; [d]Department of Medicine II, Klinikum Rechts der Isar, Technische Universität München, 81675 Munich, Germany; [e]German Cancer Research Center (DKFZ) and German Cancer Consortium, 69120 Heidelberg, Germany; and [f]Preclinical Safety, Novartis Institutes for BioMedical Research, 4056 Basel, Switzerland

Edited by Neal G. Copeland, Houston Methodist Research Institute, Houston, TX and approved February 14, 2017 (received for review December 16, 2016)

Inhibitors of double minute 2 protein (MDM2)–tumor protein 53 (TP53) interaction are predicted to be effective in tumors in which the *TP53* gene is wild type, by preventing TP53 protein degradation. One such setting is represented by the frequent *CDKN2A* deletion in human cancer that, through inactivation of *p14ARF*, activates MDM2 protein, which in turn degrades TP53 tumor suppressor. Here we used piggyBac (PB) transposon insertional mutagenesis to anticipate resistance mechanisms occurring during treatment with the MDM2-TP53 inhibitor HDM201. Constitutive PB mutagenesis in $Arf^{-/-}$ mice provided a collection of spontaneous tumors with characterized insertional genetic landscapes. Tumors were allografted in large cohorts of mice to assess the pharmacologic effects of HDM201. Sixteen out of 21 allograft models were sensitive to HDM201 but ultimately relapsed under treatment. A comparison of tumors with acquired resistance to HDM201 and untreated tumors identified 87 genes that were differentially and significantly targeted by the PB transposon. Resistant tumors displayed a complex clonality pattern suggesting the emergence of several resistant subclones. Among the most frequent alterations conferring resistance, we observed somatic and insertional loss-of-function mutations in transformation-related protein 53 (*Trp53*) in 54% of tumors and transposon-mediated gain-of-function alterations in B-cell lymphoma-extra large (*Bcl-xL*), *Mdm4*, and two *TP53* family members, resulting in expression of the TP53 dominant negative truncations *ΔNTrp63* and *ΔNTrp73*. Enhanced BCL-xL and MDM4 protein expression was confirmed in resistant tumors, as well as in HDM201-resistant patient-derived tumor xenografts. Interestingly, concomitant inhibition of MDM2 and BCL-xL demonstrated significant synergy in p53 wild-type cell lines in vitro. Collectively, our findings identify several potential mechanisms by which *TP53* wild-type tumors may escape MDM2-targeted therapy.

drug resistance | MDM2 inhibitor | piggyBac screen | cancer

Among the genes most commonly altered in human cancer, regardless of tumor type, are tumor protein 53 (*TP53*) tumor suppressor (1) and *CDKN2A* (*INK4a/ARF*) (2). The latter gene encodes two tumor suppressor proteins: p16INK4a (3), an inhibitor of cyclin D-dependent kinases that, at least in part, regulates the function of the retinoblastoma protein (RB), and p19ARF (4), a negative regulator of double minute 2 protein (MDM2) function that activates TP53, thereby inducing cell cycle arrest or apoptosis. TP53 protein levels are regulated through MDM2-mediated degradation.

Toward the goal of reactivating TP53 in cells harboring inactivating upstream pathway alterations, compounds inhibiting the interaction between MDM2 and TP53, preventing TP53 degradation, have been discovered. Such agents induce TP53 reactivation in tumors in which the TP53 gene is wild type (5–8). Although preclinical studies of such MDM2 inhibitors have demonstrated significant antitumor activity, tumors commonly relapse (9, 10).

Rapid emergence of resistance is a frequent impediment in targeted therapy, and a better understanding of resistance mechanisms could be beneficial to patient survival through the identification of rational combinations and second-line therapies. In this study, we sought to understand which genes might function as key drivers of resistance to MDM2-TP53 inhibition. We chose to study resistance to HDM201, a highly specific, murine-compatible, and potent small-molecule inhibitor of the TP53-MDM2 protein–protein interaction (9, 11), which is structurally similar to a new class of inhibitors based on an imidazopyrrolidinone scaffold (12). HDM201 has recently entered Phase 1 clinical trials in cancer patients.

Transposon-based mutagenesis has been widely used to identify candidate cancer genes in various types of cancers (13–16) and can generate both loss-of-function (LOF) and gain-of-function (GOF) genetic events. In several studies, this method also has been used to characterize resistance mechanisms in vitro (17–19) and in mice

Significance

Emergence of resistance to targeted therapy constitutes a limitation to long-term clinical benefits in many instances. To anticipate potential mechanisms of resistance to double minute 2 protein (MDM2) inhibitors, we performed a piggyBac insertional mutagenesis screen in a cohort of allografts with an underlying *CDKN2A* deletion, in the presence and absence of the MDM2 inhibitor HDM201. Among the most frequent events conferring resistance, we found several mechanisms converging on direct or indirect loss-of-function inactivation of tumor protein 53 (TP53), as well as activation of the antiapoptotic B-cell lymphoma-extra large (*Bcl-xL*) gene. Importantly, our findings were confirmed in patient-derived xenograft models, underlining the benefit of large-scale in vivo forward genetic screening to identify potential resistance mechanisms to targeted therapeutics.

Author contributions: E.A.C., A. Gembarska, A.K., M.M., W.R.S., F.H., and M.R.J. designed research; E.A.C., A. Gembarska, E.M., C.E., and V.R. performed research; E.A.C., E.Y.D., M.W., R.T., J.L., R.R., S.J., and S.F. contributed new reagents/analytic tools; E.A.C., A. Gembarska, E.Y.D., E.M., M.W., R.T., A.d.W., L.B., A.K., E.S., A. Grevot, P.M., M.M., and M.R.J. analyzed data; and E.A.C., E.Y.D., W.R.S., F.H., and M.R.J. wrote the paper.

Conflict of interest statement: This research was funded by Novartis, Inc., which employed most of the authors at the time when the study was performed. A patent has been filed on "combinations of MDM2 and BCL-XL inhibitors." The authors declare no other competing financial interests.

This article is a PNAS Direct Submission.

[1]To whom correspondence should be addressed. Email: emilie.chapeau@novartis.com.

[2]A. Gembarska and E.Y.D. contributed equally to this work.

This article contains supporting information online at www.pnas.org/lookup/suppl/doi:10.1073/pnas.1620262114/-/DCSupplemental.

(20). Consequently, we conducted a large-scale transposon-based insertional mutagenesis screen to investigate the resistance to HDM201 in mice. Tumor-prone *Arf* null mice (21), in which TP53 is suppressed by MDM2, were crossed with mice carrying the piggyBac (PB) transposon system (15), composed of the PB DNA transposon ATP2-S1 (ATP2) and a constitutively expressed PB transposase from the *Rosa26* locus (RosaPB) (15). The PB transposon system has cut-and-paste properties without leaving undesired footprints, and the ability to integrate randomly throughout the entire genome. Monitoring emerging resistance in spontaneous tumors is technically challenging, and thus the screening was performed after these tumors were transplanted into the flanks of recipient mice and these allografted tumors were expanded in larger cohorts of animals. This approach allowed for the study of a substantially larger number of resistant tumors.

The results from our screen shed light on the diversity of resistance mechanisms encountered on disruption of the TP53-MDM2 interaction. They also support the use of transposon-based mutagenesis as a powerful tool for the identification of novel resistance genes and mechanisms in genetically modified mouse models, and constitute the first in vivo resistance screen for TP53-MDM2 inhibition. Our insights may lead to better combination strategies in patients with TP53 wild-type tumors who experience relapse while being treated with MDM2-TP53 inhibitors.

Results

PB-Induced Spontaneous Tumors in the *Arf*$^{-/-}$ Background and Derived Allograft Models. To generate a set of tumors suitable for assessing MDM2 inhibitor sensitivity and the emergence of resistance, we crossed mice to combine genetic components of the constitutive PB system bearing ATP2-S1 (ATP2) and *Rosa26*-transposase (RosaPB) (15) with an *Arf* null allele (Fig. S1*A*) deficient for *p19Arf,* a tumor suppressor and TP53 regulator (21, 22). Consistent with a previously described Sleeping Beauty mutagenesis in an *Arf*$^{-/-}$ background (23), PB mutagenesis significantly decreased the time to morbidity in our cohort of 295 *Arf*$^{-/-}$ mice (Fig. 1*A*); however, the tumor spectrum in *Arf*$^{-/-}$ mice with PB mutagenesis was altered compared with that found in *Arf*$^{-/-}$-only mice (Fig. S1 *B–D*). Histopathological analyses of 331 tumors showed that constitutive PB together with *Arf* deletion, in a mixed genetic background, leads to a broad range of pathologies, including hematologic tumors, sarcomas, and, to a lesser extent, carcinomas and brain tumors (Fig. S1*E*).

To enable drug testing using the *Arf*$^{-/-}$ PB model, we serially transplanted tumors as for human patient-derived xenografts (9). To this end, we implanted fragments of spontaneous RosaPB/+;ATP2/+;Arf$^{-/-}$ tumors s.c. in athymic nude mice. Once an allograft tumor grew, it was further expanded in 20–60 immunodeficient mice (Fig. S2*A*). The overall rate of successful engraftment was 72.4%, and 21 independent allograft models, including 8 lymphomas, 6 sarcomas, and 5 medulloblastomas (Fig. S2*B*), were used to study resistance to HDM201.

Insertional Mutagenesis Landscapes in *Arf*-Deleted PB Tumors. To robustly identify genes recurrently targeted by transposons with good statistical power, we first sequenced the transposon insertion sites of 327 spontaneous tumors obtained from RosaPB/+;ATP2/+;Arf$^{-/-}$ mice. Following DNA shearing, amplicons were derived by a splinkerette PCR and sequenced from both transposon arms (24). This method allowed us to consider only the diversity counts (div counts hereinafter) within each sample; each uniquely sheared end was counted rather than all sequencing counts, thereby minimizing PCR-induced amplification effects. Using a gene-centric common insertion site (gCIS) calling method (25, 26), which identifies densities higher than predicted by chance of transposon insertions within the coding regions plus the 10-kB promoter of all RefSeq genes, we identified 2,444 CISs found in at least two tumors (Fig. 1*C* and Dataset 1). Two parameters were considered for each CIS: the number of tumor samples in which the CIS gene was targeted and the average of normalized div counts that estimate the frequency of insertion at the CIS within samples. Because each sample was deeply sequenced (at least 10^5 normalized div counts for each PB arm), CIS genes could be identified in just one sample (Fig. S3*A*).

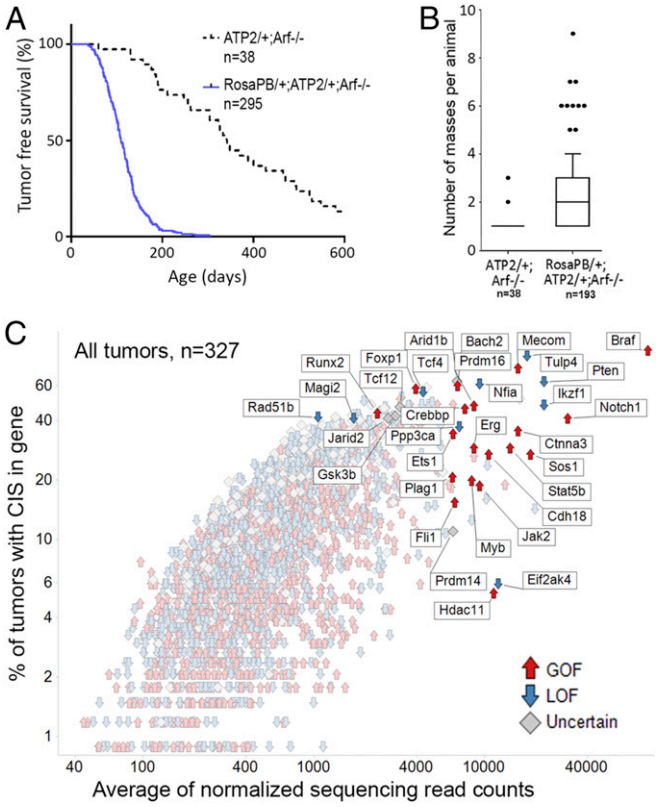

Fig. 1. Survival of RosaPB/+;ATP2/+;Arf$^{-/-}$ mice and tumoral insertional landscapes. (*A*) Survival curve (conditional survival) showing significant acceleration of disease onset with activated PB transposon ($P > 0.0001$, log-rank test). (*B*) Number of masses harvested from necropsied animals is on average significantly higher for RosaPB/+;ATP2/+;Arf$^{-/-}$ mice than for ATP2/+;Arf$^{-/-}$ mice ($P < 0.0001$, Mann–Whitney *U* test). (*C*) Genetic landscape of PB insertions in the 327 RosaPB/+;ATP2/+;Arf$^{-/-}$ tumors sequenced.

Our data from the PB transposon show negligible local hopping, consistent with a previous report (27). Indeed, although we observed a mild peak of integration at the donor site on chromosome 17, this site retained very low clonality or frequency (Fig. S4). In addition, we detected no local hopping at regions of abundant directional insertion sites, including within the *Braf* gene (Fig. S5). Consequently, we could define predictive thresholds for which oncogenes or tumor suppressor functions could be estimated (Figs. S3*B* and S5) by looking at the fraction of PB insertions in same or opposite sense as the gene. Consistent with previous Sleeping Beauty mutagenesis in the *Arf*$^{-/-}$ background (23), *Braf* was the most frequent target for transposon insertion. It was found in 90.8% of tumors, indicating that it may constitute a major cooperating pathway with Arf LOF in mice. Indeed, we found no insertions at *Braf* in PB tumors with no *Arf* deletion (data not shown). The *Braf* gene was PB-inserted between exons 8 and 12 in a directional manner (Fig. S5*A*), presumably leading to the expression of a specific constitutively active truncated protein, as described previously (23, 28). Similar human *BRAF* gene truncations or fusions have been reported in human brain, pancreatic, and prostate tumors (28–34). In some cases, the insertional landscape exhibited genetic specificities consistent with respective tumor indications (Fig. S3 *C–E*); for instance, genes commonly mutated in patients with peripheral nerve sheath cancers (MPNSTs) (35) and medulloblastomas (36–38) were also identified in our samples. *Ptch1* was among the top-five CIS genes in our medulloblastoma samples (Fig. S3*D*). *Ptch1* disruption in mouse models leads to medulloblastoma development (39).

We next sought to understand the extend of genetic drift after tumor fragment transplantation and expansion for RosaPB/+;ATP2/+;Arf$^{-/-}$ allografted tumors. Comparison of insertional patterns in a t-distributed stochastic neighbor embedding analysis, taking the div counts for each CIS into account, revealed mild genetic drifts. All tumors of the same model generally clustered together (Fig. S6).

Response and Resistance to TP53-MDM2 Inhibition in PB Allografts. Loss of *p14ARF* occurs in numerous cancers through deletion of the *CDKN2A* gene. *ARF* loss raises the MDM2 level, which in turn degrades TP53. HDM201 disrupts both human and murine TP53-MDM2 interactions, with nanomolar cellular IC_{50} values, blocking TP53 degradation (11, 12). Because of *Arf* deletion, we expected RosaPB/+;ATP2/+;Arf$^{-/-}$ transplanted tumors to respond to HDM201; however, the insertional landscapes may alter the dependency by introducing other, eventually dominant, oncogenic events (Fig. 1*B*). To assess the tumor sensitivity to HDM201, we treated 21 allograft models (Fig. S2*B*) at passage 1 (Fig. S7). After random enrollment, 139 mice were treated twice weekly with 100 mg/kg of HDM201, and 106 mice were treated with vehicle. We found a significant response rate across the 21 models (Fig. 2*A* and Fig. S7), suggesting that Arf deletion generally confers tumor dependency to MDM2 inhibitors, as predicted. Overall, only 5 out of 21 models exhibited a poor response to HDM201 and intrinsic resistance. The remaining models responded, but most tumors eventually relapsed (Figs. S2*B* and S7). In total, 6 out of 139 mice (4.3%) were potentially cured, experiencing no relapse within 60 d after the last dose. The average number of CISs per model from untreated tumors was not significantly different between the responsive and nonresponsive models. We found an average of 195 CISs per individual tumor for the responders and 202 per individual tumor for the nonresponders. This suggests that the insertional heterogeneity is likely not the reason for the lack of response to HDM201. We also could not identify specificities in the genetic patterns between nonresponsive and responsive tumors. In summary, despite a good initial response rate to HDM201 for the RosaPB/+;ATP2/+;Arf$^{-/-}$ implanted tumors, most tumors eventually became resistant.

Identification of Mechanisms of Resistance to TP53-MDM2 Inhibition by Insertional Mutagenesis. To define insertional events linked to the development of resistance to TP53-MDM2 inhibition, we subjected genomic DNA from resistant and vehicle-treated tumors to splinkerette PCR and deep sequencing to define gCIS landscapes (Dataset S2). Hierarchical clustering analysis revealed that resistant and untreated tumors of the same model had conserved insertional patterns (Fig. S6), and thus resistance did not induce a major genetic drift. A differential integration analysis identified PB target genes that were significantly enriched in 95 resistant tumors compared with 80 vehicle-treated tumors (Fig. 2*B* and Dataset S2). A total of 87 genes were identified, suggesting diversity and/or heterogeneity of the resistance mechanism; however, gene ontology/pathway analysis for these 87 genes revealed that only the TP53 pathway, including transformation-related protein 53 (*Trp53*), *Trp63*, *Trp73*, and *Mdm4*, was significantly represented. *Trp53* was the most significantly enriched gene in HDM201-resistant tumors. Variable intratumoral clonality, based on the analysis of div counts, suggested homozygous, heterozygous, or subclonal targeting (Fig. 3). The PB bidirectional pattern predicted a LOF (Fig. 4*A*). This is in line with previously reported data identifying TP53 mutagenesis as a major mechanism of resistance to TP53-MDM2 inhibitors, for either intrinsic resistance (7) or induced resistance (40–42). *Trp53* exons sequencing of all our resistant DNA samples also identified *Trp53* somatic mutations in 13 out of 95 resistant tumors (Fig. 3), in exons coding for the DNA-binding domain (12 samples), or a splice site (one sample) (Fig. 4*B*). In total, 53.7% of tumors (51 out of 95) had a *Trp53* mutation, either somatic or insertional.

Bcl2l1 was identified as the second major enriched target in HDM201-resistant tumors, with a GOF insertional pattern that did not allow distinction between expression of B-cell lymphoma-extra large (*Bcl-xL*) or *Bcl-xS* transcripts (Fig. 4*C*). However, our immunoblotting experiment demonstrated that BCL-xL protein, but not BCL-xS, was expressed in resistant tumors with transposon insertion in the *Bcl2l1* promoter (Fig. 4*D*). BCL-xL acts in the mitochondrial apoptotic pathway (43, 44), and our data suggest that the TP53-mediated proapoptotic response may be efficiently counteracted by BCL-xL expression in resistant tumors. *Mdm4* was targeted with a high-clonality GOF pattern in eight resistant tumors (Fig. 4*E*). MDM4 (also known as MDMX) is another regulator of TP53 that is structurally related to MDM2 but acts differently on TP53 by regulating its transcriptional activity independently of MDM2 or its protein level coordinately with MDM2 (45, 46). Our results thus provide evidence that *Mdm4* overexpression (Fig. 4*F*) confers resistance to selective TP53-MDM2 inhibition.

Two *Trp53* family members, *Trp63* and *Trp73*, were targeted in several HDM201-resistant tumors. Each gene of the *TP53/Trp53* family produces several isoforms owing to alternative transcription start or splicing. P2 alternative promoters produce transactivation domain-deficient proteins (ΔN) with dominant-negative functions. Heterocomplexes with ΔN forms compete off long-TA (entire transactivation domain) isoforms from their target gene promoters, thereby preventing efficient transcription (47). Our data reveal a number of HDM201-resistant tumors with unidirectional insertions in *Trp63* and *Trp73* and consistent protein overexpression (Fig. 4 *G*–*J*). Transposon insertions were located specifically near P2 promoters, suggesting the expression of truncated variants similar to *ΔNTrp73* and *ΔNTrp63*, consistent with a dominant negative function on TRP53 (47).

Overall, four genes known to regulate TRP53 activity directly or indirectly were identified as major GOF hits. TRP53 stability, transcriptional regulation, and mitochondrial apoptosis activities were targeted through MDM4, BCL-xL, ΔNTRP63, and ΔNTRP73 in 63% of tumors.

Because both MDM4 (48) and BCL-xL are known druggable targets, we next investigated whether their enhanced expression was observed in patient-derived tumor xenograft models (PDX) models. To this end, we took advantage of a cohort of previously tested breast and lung patient tumor xenograft that acquired resistance to HDM201 (9). MDM4 protein was overexpressed only in one PDX-resistant model out of 24 assessed, whereas BCL-xL overexpression was detected in five resistant human tumors (Fig. 5*A*).

BCL-xL Reduces Activity of MDM2 Inhibitors in Human TP53 Wild-Type Tumor Models. BCL-xL can be pharmacologically inhibited by the dual BCL-2/BCL-xL inhibitor ABT-263 (49) or by a BCL-xL– selective inhibitor, such as A-1155463 (50). To understand whether dual inhibition of BCL-xL and MDM2 might be beneficial across a broad spectrum of cancers, we evaluated the synergistic effects of 51 compounds with CGM097 in an in vitro viability screen on 485 cancer cell

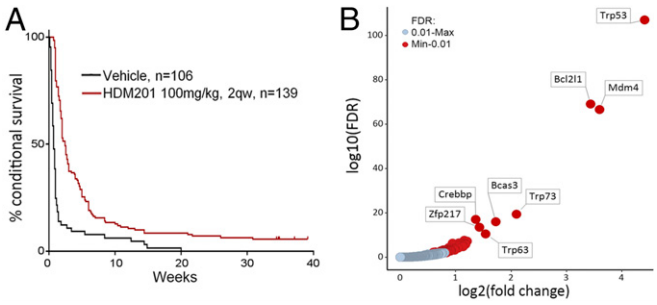

Fig. 2. Response and resistance to HDM201 TP53-MDM2 inhibitor allografted mice. (*A*) Kaplan–Meier curve representing the conditional survival of mice after the first treatment dose. All 21 RosaPB/+;ATP2/+;Arf$^{-/-}$ tumor models are combined. The median survival was 0.71 wk for vehicle-treated animals ($n = 106$) and 2.48 wk for the animals treated twice weekly ($n = 139$) ($P < 0.0001$, log-rank test). (*B*) Comparative analysis of insertional patterns between vehicle-treated tumors and tumors that emerged from HDM201-treated and -resistant tumors. The models used are listed in Fig. S2*B*. A total of 87 genes were found to be significantly differentially inserted in resistant vs. untreated tumors [false discovery rate (FDR) = 0.01].

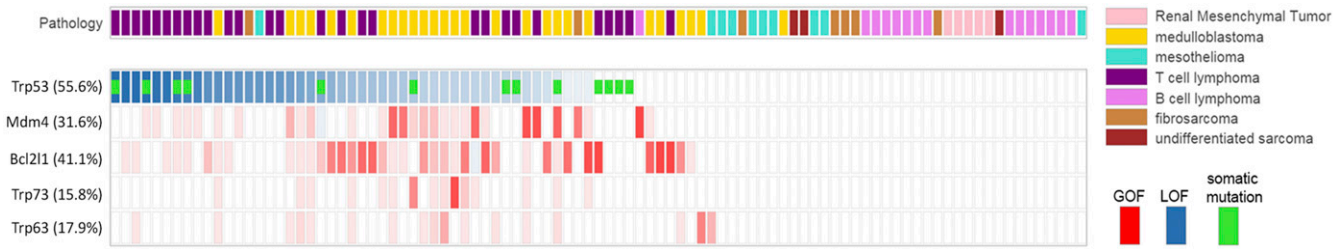

Fig. 3. Resistance mechanisms identified in HDM201-resistant tumors. Representation of major PB transposon insertions found significantly enriched in RosaPB/+;ATP2/+;Arf$^{-/-}$ HDM201-resistant implanted tumors compared with untreated tumors (n = 95 tumors with differential PB insertions). Predicted GOF or LOF transposon mutations and clonality are represented; transparency is obtained by scaling the normalized div count between 0 and 1. The presence of *Trp53* somatic mutations is indicated by a green rectangle.

lines (9, 51). Interestingly, ABT-263 was among the best combination partners with CGM097 in the 138 of these cell lines that were wild type for TP53 (Fig. S8*A*). Exposing the 485 cancer cell lines to a dose matrix of ABT-263 and CGM097, an earlier TP53-MDM2 inhibitor (5–7), revealed significant synergy in 35 out of the 138 TP53 wild-type cell lines, and no significant synergy in TP53 mutant cell lines (Fig. 5*B* and Fig. S8*B*). Collectively, these data suggest that a fraction of patients with TP53 wild-type tumors might benefit from a dual treatment with BCL-2/BCL-xL inhibitor and MDM2 inhibitor, consistent with previous observations in leukemia that combination treatment of MDM2 inhibitor and ABT-263 could achieve longer-term tumor regression (41).

To confirm that the combination effects were mediated by BCL-xL and not BCL-2 inhibition, we performed dose-matrix combination experiments with HDM201 and the BCL-xL–selective inhibitor A-1155463 (50) in two of the cell lines (SNG-M and LS-513) with relatively high BCL-xL baseline expression that responded well to a combination of CGM097 and ABT-263. As expected, we found strong synergy between HDM201 and A-1155463 in both lines (Fig. 5*C* and Fig. S9). Conversely, induced overexpression

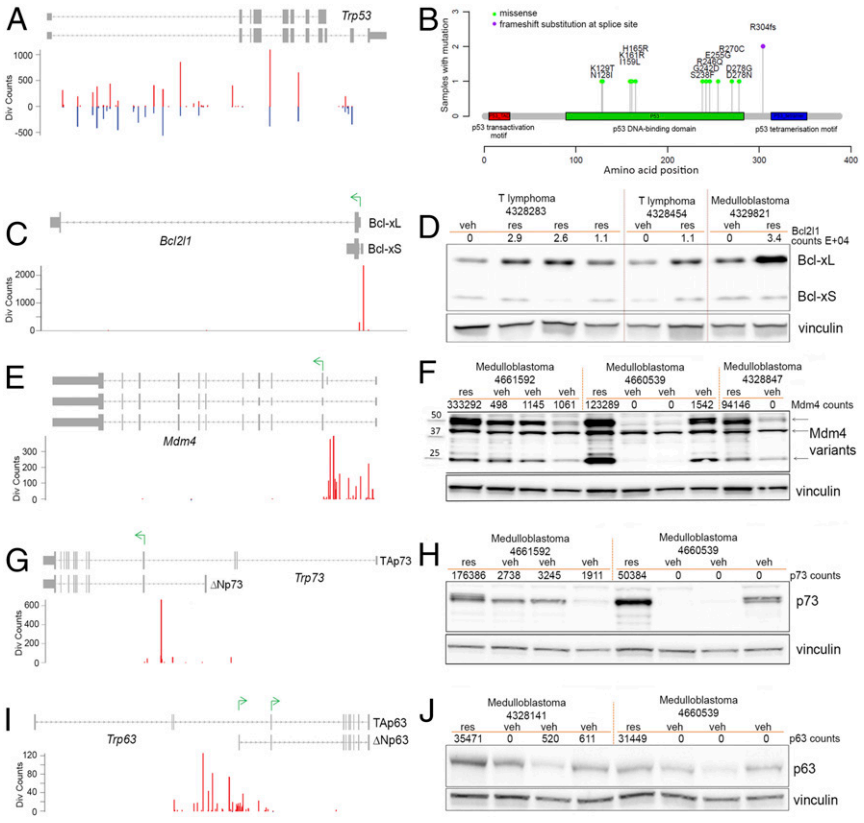

Fig. 4. Characterization of genetic modifications in HDM201-resistant tumors. (*A*, *C*, *E*, *G*, and *I*) PB insertional patterns in specific genes, from HDM201-resistant tumors. Red bars represent insertions in the same sense as the gene; blue bars, insertions in the opposite sense from the gene. (*A*) Insertional pattern in *Trp53* gene suggesting an LOF. (*B*) Somatic mutations identified on the mouse *Trp53* gene in RosaPB/+;ATP2/+;Arf$^{-/-}$ allografted tumors that are resistant to HDM201. Out of 95 tumors sequenced, 13 were found with a mutation within *Trp53* exons or splice sites. (*C*) Insertional pattern in *Bcl2l1* gene suggesting a GOF. (*D*) Western-blot analysis of tumors shows that BCL-xL is the *Bcl2l1* isoform expressed when PB insertion is found in resistant tumors. veh, vehicle-treated tumors; res, HDM201-resistant tumors. (*E*) Insertional pattern in *Mdm4* suggesting a GOF. (*F*) Western blot analysis of tumors showing that several MDM4 variants are produced when PB insertion is found in resistant tumors. (*G*) Insertional pattern in *Trp73* suggesting a GOF and production of a shorter isoform. (*H*) Western blot analysis of tumors shows that TRP73 (p73) is overexpressed in resistant tumors bearing PB insertions in *Trp73*. The protein size difference between isoforms is too small to be distinguishable. (*I*) Insertional pattern in *Trp63* suggesting a GOF and production of a shorter isoform. (*J*) Western blot analysis of tumors showing TRP63 (p63) protein levels in resistant tumors bearing PB insertions in *Trp63*. The protein size difference between isoforms is too small to be detectable.

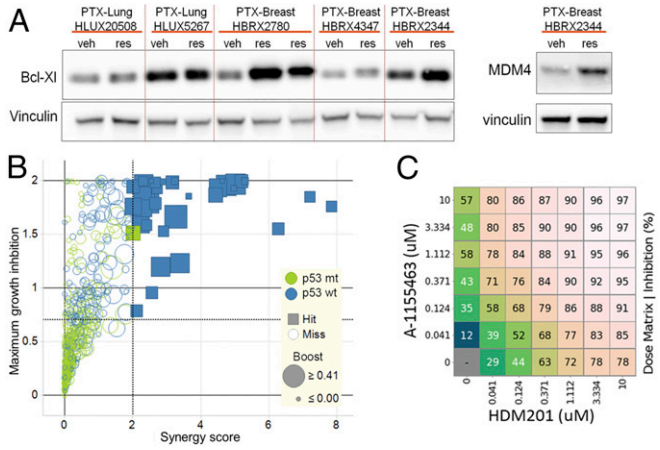

Fig. 5. Bcl-xL expression confers resistance to HDM201. (*A*) Western blot analysis showing BCL-xL and MDM4 protein expression in PDX models that acquired resistance to HDM201 or CGM097 (res) or were matched vehicle-treated (veh) (9). (*B*) Score plots for the combination of CGM097 and ABT-263 from an in vitro combination screen on 485 cancer cell lines treated with ranges of concentrations for CGM097 and ABT-263. Cell lines with no *TP53* mutation are shown in blue (p53 wt), and cell lines with *TP53* modification are shown in green (p53 mt). Boost describes the maximal growth inhibition for any combination vs. the highest single agent activity. (*C*) Synergistic effect of combinations of HDM201 TP53-MDM2 inhibitor and A-1155463 Bcl-xL inhibitor in the SNG-M cell line. Percent inhibition is shown, each number representing the average of three replicates. Gradient of colors was used for better visualization.

of BCL-xL in a metastatic melanoma TP53 wild-type cell line (WM266.4) with relatively low baseline expression of BCL-xL led to a markedly reduced sensitivity to HDM201, with a sixfold higher GI50 when BCL-xL was overexpressed (Fig. S9).

Discussion

Here we used the PB transposon system in an *Arf*-deleted mouse model to identify genes that accelerate tumorigenesis and mediate resistance to the TP53-MDM2 inhibitor HDM201. We used DNA shearing followed by splinkerette PCR and deep sequencing to allow quantification of the amplicon diversity based on the sheared end and estimation of the clonality of each tumor sample. From the 327 PB tumors in the *Arf* null background, we identified 2,444 candidate cancer genes. On average, 284 ± 145 CIS genes were identified per tumor, much more than the 15 copies carried in the ATP2 transposon (15). These results reveal the existence of substantial intertumoral and intratumoral heterogeneity; however, only 7.9% of these genes were frequently altered, with more than 20,000 normalized div counts on average per tumor, whereas the majority (92.1%) displayed low-frequency insertions and thus may be less impactful (Fig. S3*A*). Overall, the average number of CISs with high clonality was only 17.7 ± 6.6 per tumor, more consistent with Darwinian theories of evolution in tumors, where certain subclones containing a selective growth or survival advantage in comparison with others are likely to proliferate and eventually form the majority of the tumor population.

In the RosaPB/+;ATP2/+;Arf$^{-/-}$ models, no significant local transposon hopping effect was observed. The low number of background insertions allowed us to define a method to permit the prediction of GOF or LOF transposon insertions. Known oncogenes and tumor suppressor genes can be successfully predicted with our methods. In total, 952 of the CISs were predicted as GOF and 1,153 as LOF, whereas 339 could not be predicted. The most frequently targeted oncogene was a specific truncated version of the *Braf* gene that leads to constitutive activation of the protein. This is consistent with a previous report also using transposon-based mutagenesis in the Arf$^{-/-}$ background (23). The fact that *Braf* insertions were not identified in PB tumors with no *Arf* deletion (data not shown) suggests that truncated *Braf* and *Arf* LOF may cooperate in mice. Other frequently activated oncogenes were *Mecom*, *Foxp1*, and *Bach2*, whereas the major tumor suppressor genes identified included *Pten*, *Ikzf1*, *Tulp4*, and *Tcf4*, among others (Fig. S5).

We performed a screen to identify genes involved in the resistance to TP53-MDM2 inhibition. To this end, we used allografted tumors from 16 RosaPB/+;ATP2/+;Arf$^{-/-}$ tumor models sensitive to HDM201, and found 87 CIS genes significantly targeted in resistant tumors but not (or not much) in vehicle-treated tumors. Our work represents an important example of how in vivo transposon-mediated mutagenesis can be used to elucidate genetic mechanisms of cancer drug resistance. Our allograft approach facilitates sample generation used to identify novel genes and mechanisms, and the PB transposon provides a powerful tool for identifying GOF or LOF resistance mechanisms to TP53-MDM2 targeted inhibition. The general stability of PB genetic landscapes, revealed by the absence of major genetic drift across passaging or on HDM201 resistance acquisition, permits the identification of genes specifically targeted in HDM201-resistant tumors compared with vehicle-treated tumors.

Inhibition of the TP53 gene itself by mutagenesis is a known major mechanism of resistance to TP53-MDM2 inhibitors for either intrinsic resistance (7) or induced resistance (40, 42). We consistently identified not only PB mutation in the *Trp53* gene, but also somatic mutations in 13 out of 95 *Trp53* sequenced tumors (13.8%). In total, 53.7% of tumors carried a *Trp53* mutation, either somatic or transposon. The somatic mutations were likely inhibitory, found mainly in the DNA-binding domain, whereas the PB mutation pattern was consistent with an LOF. The presence of TP53 inhibitory somatic mutations revealed that PB transposon was not the sole mutagen acting in these tumors. Indeed, the ATP2-S1 PB model used here is known to carry 15 transposon copies; however, tumors generally carry larger numbers of genetic alterations (52), and succession of genetic alterations is likely required to achieve cancer progression into a resistant state. Therefore, it is plausible that PB insertions are not the only functional somatic modifications. The nature of CIS genes targeted by PB (Dataset S1) suggests that diverse genetic and epigenetic posttranslational alterations likely occur in these tumors. For instance, a number of genes known to be altered in cancer and to generate genomic instability were found to be mutated by PB, including *Rad51b*, *Rad51d*, *Atm*, *Wrn*, *Nbn*, *Mlh1*, *Msh5*, and *Pms1*, known to promote somatic mutations in human cancers (53, 54). In addition, alterations of known chromatin remodeling factors, including *Arid1b*, four different *Hdac* genes, *Brd4*, and *Eed*, may trigger epigenetic changes in these tumors.

Among the 87 CIS genes specifically identified in HDM201-resistant tumors, the most significant transposon-altered genes included those directly regulating the TP53 pathway, including *Trp53* (50%), *Mdm4* (31.9%), ΔN isoform of *Trp63* (18.1%), and ΔN isoform of *Trp73* (16%). Whereas *Trp53* PB mutations were consistent with an inhibitory pattern of transposon insertions, the other genes displayed an insertional pattern consistent with gene overexpression that was confirmed on additional analyses. Although there is previous evidence that MDM4 expression reduces sensitivity to nutlin-3 MDM2 inhibitor (55), our present unbiased genetic screen has identified MDM4 overexpression as a mechanism of resistance to an MDM2 inhibitor. Thus, specific MDM4 antagonists may provide therapeutic benefits in cases where resistance occurs by MDM4 overexpression in wild-type TP53 tumors. ΔN isoforms of *Trp73* and *Trp63* are produced by an alternative promoter and lack the transactivation domain (47). They are suspected to exhibit proto-oncogenic function and TP53 dominant-negative functions. Our findings corroborate the latter hypothesis and suggest that resistance to TP53-MDM2 inhibition may occur in some cases through TP53 inhibition by these truncated isoforms. Interestingly, *Bcl2l1* was the second most significant CIS gene enriched in HDM201-resistant tumors, after *Trp53*. Activating transposon insertions in these resistant samples led to enhanced BCL-xL protein expression. Further in vitro experiments demonstrated that BCL-xL increased expression conferred reduced sensitivity to TP53-MDM2 inhibition, whereas BCL-xL inactivation increased the response to TP53-MDM2 inhibition.

Overall, the identification of major resistant mechanisms, where the five most significant PB-targeted genes accounted for 63% of tumors, may help predict the future clinical course of patients treated with

TP53-MDM2 inhibitors. In the majority of cases, in our present models, intertumor and intratumor heterogeneity of resistance mechanisms was observed. Although we cannot assess whether insertional intratumor heterogeneity arose from independent subclones, the results from independent allografted tumors passaged from the same original tumor model suggest that subclonal heterogeneity occurs. Heterogeneity of resistance mechanisms is consistent with a clonal adaptation that occurred in the course of an evolutionary process. Subclonal heterogeneity allows dynamic tumor adaption and is generally a key cause of treatment failure (56). To our knowledge, no therapy is available to counteract TP53 mutations or expression of ΔNTP63 and ΔNTP73; currently, only MDM4 (48) and BCL-xL (49, 50) can be targeted pharmacologically. Our in vitro assays demonstrate that BCL-xL inhibition sensitized cells to HDM201 inhibition. Upfront combination therapies with such agents (57) may provide a more promising therapeutic strategy for achieving complete killing of cancers.

Materials and Methods

Detailed information on the animal experiments, tumor sequencing, mapping of insertion sequences to the mouse genome and identification of common integration sites, Western blot analyses, and cell line combination synergy testing is provided in *SI Materials and Methods*. All animal studies were conducted in accordance with the Kantonales Veterinäramt Basel-Stadt (licenses BS-2604 and BS-1763) and in strict adherence to guidelines of the Eidgenössisches Tierschutzgesetz and the Eidgenössische Tierschutzverordnung, Switzerland.

ACKNOWLEDGMENTS. We thank Allan Bradley for sharing the piggyBac mice and advice; Melanie Heinlein, Lea Buehler, Baptiste Gouyou, Heidi Poulet, and Fritz Wenger for helping with the mouse and histology experiments; Daniel Breustedt and team for breeding mice; Edward Oakeley, Ulrike Naumann, Moriko Ito, Sabine Zumstein-Mecker, and David Ruddy for optimizing and running the sequencing experiments; Pedro Marques Ramos and Michael Stadler for discussions and bioinformatics analyses; and Mark Stump for his contribution to the combination screen.

1. Hollstein M, et al. (1994) Database of p53 gene somatic mutations in human tumors and cell lines. *Nucleic Acids Res* 22(17):3551–3555.
2. Ruas M, Peters G (1998) The p16INK4a/CDKN2A tumor suppressor and its relatives. *Biochim Biophys Acta* 1378(2):F115–F177.
3. Serrano M, Hannon GJ, Beach D (1993) A new regulatory motif in cell-cycle control causing specific inhibition of cyclin D/CDK4. *Nature* 366(6456):704–707.
4. Sherr CJ (2006) Divorcing ARF and p53: An unsettled case. *Nat Rev Cancer* 6(9):663–673.
5. Holzer P, et al. (2015) Discovery of a dihydroisoquinolinone derivative (NVP-CGM097): A highly potent and selective MDM2 inhibitor undergoing phase 1 clinical trials in p53wt tumors. *J Med Chem* 58(16):6348–6358.
6. Jeay S, et al. (2015) A distinct p53 target gene set predicts for response to the selective p53-HDM2 inhibitor NVP-CGM097. *eLife* 4:4.
7. Weisberg E, et al. (2015) Inhibition of wild-type p53-Expressing AML by the novel small molecule HDM2 inhibitor CGM097. *Mol Cancer Ther* 14(10):2249–2259.
8. Zhao Y, Aguilar A, Bernard D, Wang S (2015) Small-molecule inhibitors of the MDM2-p53 protein–protein interaction (MDM2 inhibitors) in clinical trials for cancer treatment. *J Med Chem* 58(3):1038–1052.
9. Gao H, et al. (2015) High-throughput screening using patient-derived tumor xenografts to predict clinical trial drug response. *Nat Med* 21(11):1318–1325.
10. Townsend EC, et al. (2016) The public repository of xenografts enables discovery and randomized phase ii-like trials in mice. *Cancer Cell* 29(4):574–586.
11. Hofmann F (2016) Small molecule HDM2 inhibitor HDM201. *Proceedings of the 107th Annual Meeting of the American Association for Cancer Research. Cancer Res* 76(14; Suppl):6291.
12. Furet P, et al. (2016) Discovery of a novel class of highly potent inhibitors of the p53-MDM2 interaction by structure-based design starting from a conformational argument. *Bioorg Med Chem Lett* 26(19):4837–4841.
13. Copeland NG, Jenkins NA (2010) Harnessing transposons for cancer gene discovery. *Nat Rev Cancer* 10(10):696–706.
14. Moriarity BS, Largaespada DA (2015) Sleeping Beauty transposon insertional mutagenesis based mouse models for cancer gene discovery. *Curr Opin Genet Dev* 30:66–72.
15. Rad R, et al. (2010) PiggyBac transposon mutagenesis: A tool for cancer gene discovery in mice. *Science* 330(6007):1104–1107.
16. Rad R, et al. (2015) A conditional piggyBac transposition system for genetic screening in mice identifies oncogenic networks in pancreatic cancer. *Nat Genet* 47(1):47–56.
17. Chen L, et al. (2013) Transposon activation mutagenesis as a screening tool for identifying resistance to cancer therapeutics. *BMC Cancer* 13:93.
18. Pandzic T, et al. (2016) Transposon mutagenesis reveals fludarabine-resistance mechanisms in chronic lymphocytic leukemia. *Clin Cancer Res* 22(24):6217–6227.
19. Tsutsui M, et al. (2015) Comprehensive screening of genes resistant to an anticancer drug in esophageal squamous cell carcinoma. *Int J Oncol* 47(3):867–874.
20. Perna D, et al. (2015) BRAF inhibitor resistance mediated by the AKT pathway in an oncogenic BRAF mouse melanoma model. *Proc Natl Acad Sci USA* 112(6):E536–E545.
21. Kamijo T, et al. (1997) Tumor suppression at the mouse INK4a locus mediated by the alternative reading frame product p19ARF. *Cell* 91(5):649–659.
22. Kamijo T, Bodner S, van de Kamp E, Randle DH, Sherr CJ (1999) Tumor spectrum in ARF-deficient mice. *Cancer Res* 59(9):2217–2222.
23. Collier LS, Carlson CM, Ravimohan S, Dupuy AJ, Largaespada DA (2005) Cancer gene discovery in solid tumours using transposon-based somatic mutagenesis in the mouse. *Nature* 436(7048):272–276.
24. Friedrich MJ, et al. (2017) Genome-wide transposon screening and quantitative insertion site sequencing for cancer gene discovery in mice. *Nat Protoc* 12(2):289–309.
25. Bard-Chapeau EA, et al. (2014) Transposon mutagenesis identifies genes driving hepatocellular carcinoma in a chronic hepatitis B mouse model. *Nat Genet* 46(1):24–32.
26. Brett BT, et al. (2011) Novel molecular and computational methods improve the accuracy of insertion site analysis in Sleeping Beauty-induced tumors. *PLoS One* 6(9):e24668.
27. Liang Q, Kong J, Stalker J, Bradley A (2009) Chromosomal mobilization and reintegration of Sleeping Beauty and piggyBac transposons. *Genesis* 47(6):404–408.
28. Jones DT, et al. (2008) Tandem duplication producing a novel oncogenic BRAF fusion gene defines the majority of pilocytic astrocytomas. *Cancer Res* 68(21):8673–8677.
29. Chen SH, et al. (2016) Oncogenic BRAF deletions that function as homodimers and are sensitive to inhibition by RAF dimer inhibitor LY3009120. *Cancer Discov* 6(3):300–15.
30. Lin A, et al. (2012) BRAF alterations in primary glial and glioneuronal neoplasms of the central nervous system with identification of 2 novel KIAA1549:BRAF fusion variants. *J Neuropathol Exp Neurol* 71(1):66–72.
31. Palanisamy N, et al. (2010) Rearrangements of the RAF kinase pathway in prostate cancer, gastric cancer and melanoma. *Nat Med* 16(7):793–798.
32. Ramkissoon LA, et al. (2013) Genomic analysis of diffuse pediatric low-grade gliomas identifies recurrent oncogenic truncating rearrangements in the transcription factor MYBL1. *Proc Natl Acad Sci USA* 110(20):8188–8193.
33. Ren G, et al. (2012) Identification of frequent BRAF copy number gain and alterations of RAF genes in Chinese prostate cancer. *Genes Chromosomes Cancer* 51(11):1014–1023.
34. Schindler G, et al. (2011) Analysis of BRAF V600E mutation in 1,320 nervous system tumors reveals high mutation frequencies in pleomorphic xanthoastrocytoma, ganglioglioma and extra-cerebellar pilocytic astrocytoma. *Acta Neuropathol* 121(3):397–405.
35. Lee W, et al. (2014) PRC2 is recurrently inactivated through EED or SUZ12 loss in malignant peripheral nerve sheath tumors. *Nat Genet* 46(11):1227–1232.
36. Jones DT, et al. (2012) Dissecting the genomic complexity underlying medulloblastoma. *Nature* 488(7409):100–105.
37. Pugh TJ, et al. (2012) Medulloblastoma exome sequencing uncovers subtype-specific somatic mutations. *Nature* 488(7409):106–110.
38. Robinson G, et al. (2012) Novel mutations target distinct subgroups of medulloblastoma. *Nature* 488(7409):43–48.
39. Genovesi LA, et al. (2013) Sleeping Beauty mutagenesis in a mouse medulloblastoma model defines networks that discriminate between human molecular subgroups. *Proc Natl Acad Sci USA* 110(46):E4325–E4334.
40. Hoffman-Luca CG, et al. (2015) Significant differences in the development of acquired resistance to the MDM2 inhibitor SAR405838 between in vitro and in vivo drug treatment. *PLoS One* 10(6):e0128807.
41. Hoffman-Luca CG, et al. (2015) Elucidation of acquired resistance to Bcl-2 and MDM2 inhibitors in acute leukemia in vitro and in vivo. *Clin Cancer Res* 21(11):2558–2568.
42. Wanzel M, et al. (2016) CRISPR-Cas9-based target validation for p53-reactivating model compounds. *Nat Chem Biol* 12(1):22–28.
43. Amaral JD, Xavier JM, Steer CJ, Rodrigues CM (2010) The role of p53 in apoptosis. *Discov Med* 9(45):145–152.
44. Green DR, Kroemer G (2009) Cytoplasmic functions of the tumour suppressor p53. *Nature* 458(7242):1127–1130.
45. Pant V, Lozano G (2014) Limiting the power of p53 through the ubiquitin proteasome pathway. *Genes Dev* 28(16):1739–1751.
46. Wade M, Li YC, Wahl GM (2013) MDM2, MDMX and p53 in oncogenesis and cancer therapy. *Nat Rev Cancer* 13(2):83–96.
47. Wei J, Zaika E, Zaika A (2012) p53 Family: Role of protein isoforms in human cancer. *J Nucleic Acids* 2012:687359.
48. Zak K, et al. (2013) Mdm2 and MdmX inhibitors for the treatment of cancer: A patent review (2011-present). *Expert Opin Ther Pat* 23(4):425–448.
49. Tse C, et al. (2008) ABT-263: A potent and orally bioavailable Bcl-2 family inhibitor. *Cancer Res* 68(9):3421–3428.
50. Leverson JD, et al. (2015) Exploiting selective BCL-2 family inhibitors to dissect cell survival dependencies and define improved strategies for cancer therapy. *Sci Transl Med* 7(279):279ra40.
51. Lehár J, et al. (2009) Synergistic drug combinations tend to improve therapeutically relevant selectivity. *Nat Biotechnol* 27(7):659–666.
52. Alexandrov LB, et al.; Australian Pancreatic Cancer Genome Initiative; ICGC Breast Cancer Consortium; ICGC MMML-Seq Consortium; ICGC PedBrain (2013) Signatures of mutational processes in human cancer. *Nature* 500(7463):415–421.
53. Lange SS, Takata K, Wood RD (2011) DNA polymerases and cancer. *Nat Rev Cancer* 11(2):96–110.
54. Wood RD, Mitchell M, Lindahl T (2005) Human DNA repair genes, 2005. *Mutat Res* 577(1-2):275–283.
55. Patton JT, et al. (2006) Levels of HdmX expression dictate the sensitivity of normal and transformed cells to Nutlin-3. *Cancer Res* 66(6):3169–3176.
56. Lipinski KA, et al. (2016) Cancer evolution and the limits of predictability in precision cancer medicine. *Trends Cancer* 2(1):49–63.
57. Horn T, et al. (2016) High-order drug combinations are required to effectively kill colorectal cancer cells. *Cancer Res* 76(23):6950–6963.